Nanoscale Horizons

ROYAL SOCIETY OF CHEMISTRY

COMMUNICATION

View Article Online
View Journal

Cite this: DOI: 10.1039/d5nh00426h

Received 18th June 2025,
Accepted 19th November 2025

DOI: 10.1039/d5nh00426h

rsc.li/nanoscale-horizons

Significant difference in charge transfer at steps on Ag(100) and Cu(100) surfaces revealed by field emission resonance

Hung-Lung Huang,[b] Shin-Ming Lu,[a] Horng-Tay Jeng,*[bac] Ho-Hsiang Chang,[a] Wen-Yuan Chan[ad] and Wei-Bin Su*[a]

We employ field emission resonance (FER) to observe the Smoluchowski effect on Ag(100) and Cu(100) surfaces, which is a charge transfer phenomenon, leading to electric dipole formation at surface steps. On Ag(100), pronounced charge transfer results in a discontinuity in FER energies at step sites. In contrast, this discontinuity is absent on Cu(100), indicating that the Smoluchowski effect is negligible. Density functional theory calculations confirm this significant difference in charge transfer at the step. By analyzing FER energies using the triangular potential model, we extract the spatial variation of the work function around the step on both surfaces. Our results for Cu(100) demonstrate that a reduction in the work function can occur even without a step electric dipole, contrary to the widely accepted explanation that the Smoluchowski effect reduces the work function. Furthermore, while it is generally accepted that as charge transfer occurs, local negative (positive) surface charge raises (lowers) the work function, our results for Ag(100) reveal the opposite trend. Additionally, the extracted work function enables spatially resolving the positive and negative charge densities within a step electric dipole, which has not yet been achieved using other local probe techniques.

New concepts

By observing the Smoluchowski effect on the Ag(100) surface, we demonstrate that field emission resonance (FER) spectroscopy is highly sensitive to the surface charge, as it enables spatial resolution of the positive and negative charge densities within the step electric dipole, a capability beyond the reach of other local probe techniques. The vacuum level variation around the surface step, extracted from FER spectra, reveals a new concept: the local work function change induced by charge transfer originates from Fermi level alignment, rather than from a modification of the surface dipole. We also show that the Smoluchowski effect is negligible on the Cu(100) surface; nevertheless, a local work function reduction near the step is still observed. This finding is inconsistent with the long-standing notion that the step electric dipole accounts for the work function reduction with increasing step density. Since FER spectroscopy allows local probing of the polarity and distribution of surface charge, we expect that it will become a powerful tool for probing atomic-scale electrostatics, charge transfer across lateral interfaces, and charge distribution in edge states.

1. Introduction

Charge transfer is a ubiquitous process that occurs at the interface where two different materials come into contact. In systems involving organic molecules on metallic substrates, charge transfer can significantly alter the physical and chemical properties of the molecules compared to their behavior in the solution phase. These alterations include molecular conformational distortions upon adsorption,[1,2] substrate-mediated interactions,[3] unique chemical reaction pathways,[4] and the emergence of molecular Kondo resonances.[5,6] Charge transfer also serves as a fundamental mechanism in contact electrification, which plays a crucial role in the development of triboelectric nanogenerators.[7] In the case where both materials are metals, charge transfer leads to the formation of a contact potential that is linearly proportional to the difference in their work functions. This principle underpins scanning Kelvin probe microscopy (SKPM),[8] a technique that enables high spatial resolution mapping of the surface morphology and the local work function.

Steps, an inherent structure of any crystalline surface, exhibit unique properties. For instance, surface steps can substantially influence heterogeneous catalysis[9] and epitaxial growth.[10] From a technological perspective, faceting of stepped surfaces holds promise as platforms for fabricating nanostructures using a "bottom-up" approach.[11,12] On an atomic scale,

[a] Institute of Physics, Academia Sinica, Nankang, Taipei, 115201, Taiwan. E-mail: wbsu@phys.sinica.edu.tw
[b] Department of Physics, National Tsing Hua University, Hsinchu, 30013, Taiwan. E-mail: jeng@phys.nthu.edu.tw
[c] Physics Division, National Center for Theoretical Sciences, Hsinchu, 30013, Taiwan
[d] Department of Electronic Engineering, Minghsin University of Science and Technology, Hsinchu, Taiwan

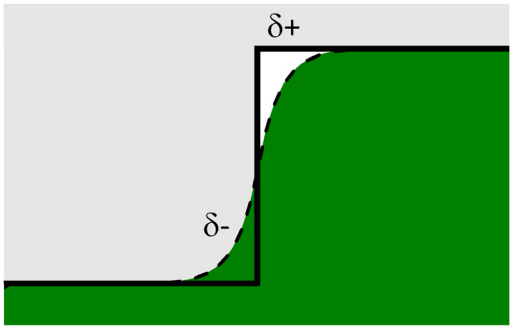

Fig. 1 Schematic illustration of the Smoluchowski effect, representing the charge transfer of electron density from the upper step edge to the step base.

the diffusion of a single atom across a step differs from its motion on a terrace due to the additional Ehrlich–Schwoebel barrier.[13,14] In 1941, Smoluchowski theoretically demonstrated charge transfer at step sites, characterized by a flow of electron density from the upper step edge to the step base, creating a local step electric dipole (SED),[15] as illustrated in Fig. 1. Subsequent studies showed experimental evidence for the existence of the SED. For example, Besocke *et al.* observed a reduction in the work function with increasing step density,[16] which was attributed to the SED. Later, local probe techniques, such as scanning tunneling microscopy (STM)[17] and SKPM,[18] provided further support by allowing the work function changes near step sites to be observed. However, direct detection of the positive charge at the upper step edge and the negative charge at the step base has remained elusive with these techniques. To spatially resolve the charge distribution within the SED, Park *et al.*[19] utilized a combination of STM and atomic force microscopy to measure the electrostatic force acting on a biased STM tip positioned at the upper step edge. The polarity-dependent changes in the electrostatic force indirectly revealed the presence of the positive charge. However, the negative charge at the step base remains unobservable.

In STM, when a bias voltage is applied such that the Fermi level of the tip becomes higher than the vacuum level of the sample, electron tunneling in the junction transitions into field emission. Because the wavelength of the field-emitted electrons is comparable to the tip–surface separation, quantized standing-wave states are formed in the junction. As a result, the field emission current oscillates with increasing bias voltage, a phenomenon known as field emission resonance (FER),[20] which can be observed using *Z*–*V* (distance–voltage) spectroscopy in STM.[21,22] Although FER originates from the quantized electronic states in the vacuum gap, previous studies[23–42] have demonstrated that its characteristics, including resonance energy, intensity, linewidth, and peak number can reflect the physical properties of both the surface and the STM tip.

In this work, we observed FER around monoatomic steps on Ag(100) and Cu(100) surfaces. On both surfaces, we discovered a phenomenon where the FER energy shifts upward as the upper step edge (USE) is approached, whereas it shifts downward near the step base (SB). While the energy shifts near the SB are comparable for both surfaces, the energy shift near the USE on Ag(100) is substantially larger than that on Cu(100) by an order of magnitude. This pronounced difference causes the FER spectra around the step on Ag(100) to exhibit an energy discontinuity for FER peaks of the same order, which is absent on Cu(100). We suggest that this notable distinction arises from significant charge transfer at the step on Ag(100), resulting in a much stronger SED. Our density functional theory (DFT) calculations corroborate this marked difference, indicating that the Smoluchowski effect is strongly dependent on the material's electronic properties. Since FER spectroscopy enables probing of the surface charge, the associated variations in the surface potential can be evaluated accordingly.

2. Methods

2.1 STM measurements

In the experiment, clean Ag(100) and Cu(100) were prepared using ion sputtering followed by annealing at 600 °C for several cycles. An ultra-high-vacuum STM operated at 5 K was used to observe FER. PtIr tips were used to perform *Z*–*V* spectroscopy combined with a lock-in technique to observe FER, in which a dither voltage of 30 mV was added at a frequency of 1 kHz to the bias voltage.

2.2 DFT calculations

First-principles calculations are performed using the local density approximation (LDA) based on density functional theory (DFT)[43,44] as implemented using the Vienna *ab initio* simulation package (VASP).[45–47] The large 16 × 1 × 6 supercell with a size of 45.23 Å × 2.83 Å × 36.99 Å (40.89 Å × 2.56 Å × 34.88 Å) containing 184 atoms is used in the slab model method for simulating the monoatomic step on (100) surface for Ag (Cu) (Fig. S1). To obtain convergent results, the slab thickness for the high (low) terrace is 12 (11) layers with the vacuum thickness of 15 Å to eliminate the interaction between the bottom and top surfaces. The convergence test for the slab thickness is shown in the SI (Fig. S2). Similarly, to avoid interactions between adjacent step edges, a terrace width four times the lattice constant (eight atoms) of over 20 Å is used.[48] The lattice constants of 3.9978 Å and 3.6145 Å given from the fully structural relaxation of Ag and Cu bulk structures are in good agreement with experimental lattice constants of 4.079 Å and 3.598 Å,[49] respectively. To reduce structural complexity and computational time, the atomic structures of the step surface are derived from the relaxed bulk structures with the self-consistent total energy calculations converged less than 10^{-9} eV per supercell. The out-of-plane dipole corrections are included in the calculations to prevent errors from dipole moments caused by creating the surfaces. 1 × 11 × 1 ***k***-mesh with a cut-off energy of 312 eV is sufficient for obtaining qualitatively reasonable results consistent with experimental data. Neither the spin polarizations nor the spin–orbit interactions are considered for these nonmagnetic and non-heavy elements.

3. Results and discussion

Fig. 2(a) shows an STM image of the Ag(100) surface, where the surface is composed of a high terrace (marked by H) and a low terrace (marked by L) separated by a monoatomic step. Along the 250 Å-long dashed line crossing the step in Fig. 2(a), we took an FER spectrum every 2 Å. Fig. 2(b) presents the FER spectrum at the start point (marked by o), with the numbers indicating the orders of FER peaks. Fig. 2(c) displays an intensity map of the FER spectra along the line, with spectral intensities represented by a color scale. The line profile crossing the monoatomic step is shown at the bottom, indicating that the USE is approximately at 122 Å. The FER peaks appear in the red and white regions. The mapping contrast shows a prominent variation for all FER peaks near the step. Consequently, the FER spectra for positions ranging from 104 to 128 Å around the step are displayed for closer inspection in Fig. 2(d), with the corresponding positions marked on the right-hand side.

First, let us examine the first-order FER peak (FER1) at different positions. As indication by the triangles in Fig. 2(d), FER1 energy is not constant. Instead, as the SB or USE is approached, the FER1 energy shifts toward lower energy on the low terrace and higher energy on the high terrace. This opposing behavior is also observed for the second-order FER peak (FER2), indicating that both FER1 and FER2 energies are discontinuous at the step. Notably, FER1 on the low terrace ($FER1_{low}$) and FER1 on the high terrace ($FER1_{high}$) coexist in the FER spectra at positions between 116 Å and 120 Å. These positions, marked by a dashed rectangle and highlighted in the inset, reveal that FER electrons emit to the low terrace when the bias voltage corresponds to $FER1_{low}$, but switch to the high terrace when the bias voltage corresponds to $FER1_{high}$. Similarly, at positions between 114 Å and 118 Å, two FER2 peaks are observed. Due to the energy discontinuity, the mapping in Fig. 2(c) shows a discontinuous contrast near the step for FER peaks of the same order, except for the zeroth order. For higher-order FER peaks (order numbers greater than two), the peak energy of n-th order on the high terrace smoothly connects with that of $(n+1)$-th order on the low terrace. This progression is clearly illustrated in Fig. 2(d), indicated by the triangles.

We conducted the same experiment on the Cu(100) surface. Fig. 2(e) shows the FER spectrum at the start point (the STM image with the step is not shown). The intensity evolution along a line crossing a step is presented in the mapping in Fig. 2(f), where the line profile indicates that the USE is approximately at 130 Å. In contrast to Fig. 2(c), however, Fig. 2(f) reveals a prominent difference: the contrast discontinuity at the step is absent. Fig. 2(g) displays FER spectra at positions ranging from 116 to 140 Å around the step. The

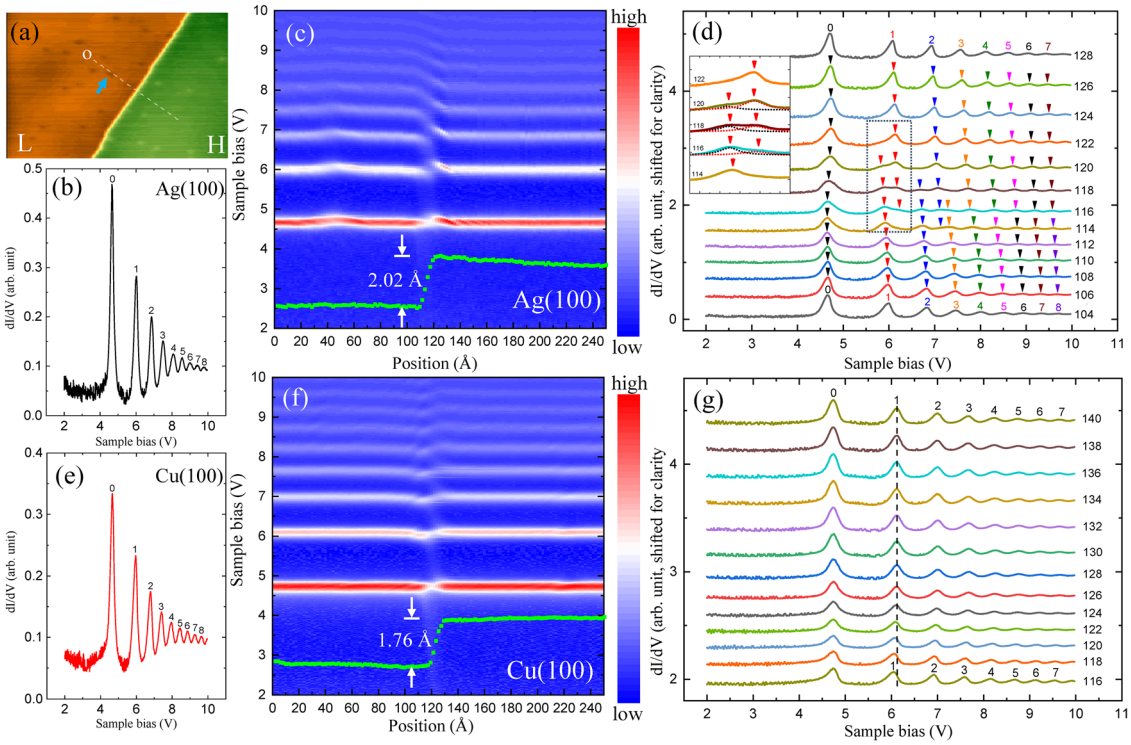

Fig. 2 (a) STM image showing a step on the Ag(100) surface. (b) FER spectrum at the starting point (marked "o") of a dashed line in (a). (c) Intensity mapping of FER spectra acquired along the dashed line crossing the step at a current of 1 nA, with the corresponding line profile shown at the bottom. (d) FER spectra showing peaks (marked by numbers) for positions from 104 to 128 Å around the step. Inset: Enlarged view of the region within the dashed rectangle, highlighting two FER1 peaks at positions from 116 to 120 Å. (e) FER spectrum at the starting point of a line crossing a step on the Cu(100) surface. (f) Intensity mapping of FER spectra at a current of 0.5 nA on the Cu(100) surface, including the corresponding line profile across the step. (g) FER spectra for positions from 116 to 140 Å around the step. A dashed line indicates the FER1 energy at the position of 140 Å.

dashed line marks the FER1 energy at the 140-Å position, showing that FER1 exhibits only a slight energy shift across the step. FER peaks of higher orders demonstrate a similar behavior.

However, on the (100) surface, the step orientations may be either ⟨011⟩ or ⟨010⟩. It remains unclear whether this substantial difference arises from the step orientation. To address this, we deliberately searched for regions on the Ag(100) and Cu(100) surfaces where the steps of both orientations coexisted and conducted the same experiments in those regions (Fig. S3 and S4). The results closely resemble the mappings shown in Fig. 2(c) and (f), suggesting that the pronounced disparity between the mappings is not attributable to the step orientation.

According to the line profiles in Fig. 2(c) and (f), the step heights on Ag(100) (2.02 Å) and Cu(100) (1.76 Å) are comparable. Thus, the step height is unlikely to be the cause of the notable disparity, where the FER energy discontinuity is observed on Ag(100) but is absent on Cu(100) at the step site. Instead, it is likely that the much stronger Smoluchowski effect on Ag(100) is the primary cause of this difference. To test this hypothesis, we performed DFT calculations.

As detailed in the Methods section, Fig. 3(a) shows the constructed supercell slab models of Ag- and Cu-stepped surfaces, where *a* and *c* correspond to the ⟨011⟩ and ⟨100⟩ directions of the face centered cubic bulk structure, respectively. Fig. 3(b) and (c) present the calculated charge density distribution within 0.5 eV below the Fermi level of Ag and Cu, respectively. As can be clearly seen, Ag demonstrates a much more diffusive 4d electron density distribution in comparison with the significantly localized 3d electron picture of Cu, particularly at the surface. For the Ag case, attracted by in-plane atoms, the electron cloud expands laterally even to the neighboring site forming the continuous distribution over several Ag atoms. This is in strong contrast to the well-separated electron cloud in the Cu case. It is also observed that surface charge on both Ag and Cu tends to distort inward the surface, showing anisotropic distributions along the surface normal direction.

Fig. 3(d) shows zoomed-in plots of the red and blue dashed rectangle regions in Fig. 3(b), allowing a clear comparison of charge redistributions on the Ag-stepped surface. As shown in Fig. 3(d), the surface charge density of Ag exhibits a pronounced distortion along the *z*-direction, with the maximum electron concentration shifted deeper into the surface. The electron density distribution varies notably along with its distance from the step edge. Furthermore, the charge density at Ag surface sites reveals a remarkable double-peak distribution along the *z*-axis, especially at sites 3 and 4. Such a step-affected charge redistribution leads to the distinct behavior observed in experimental measurements. It can also be seen

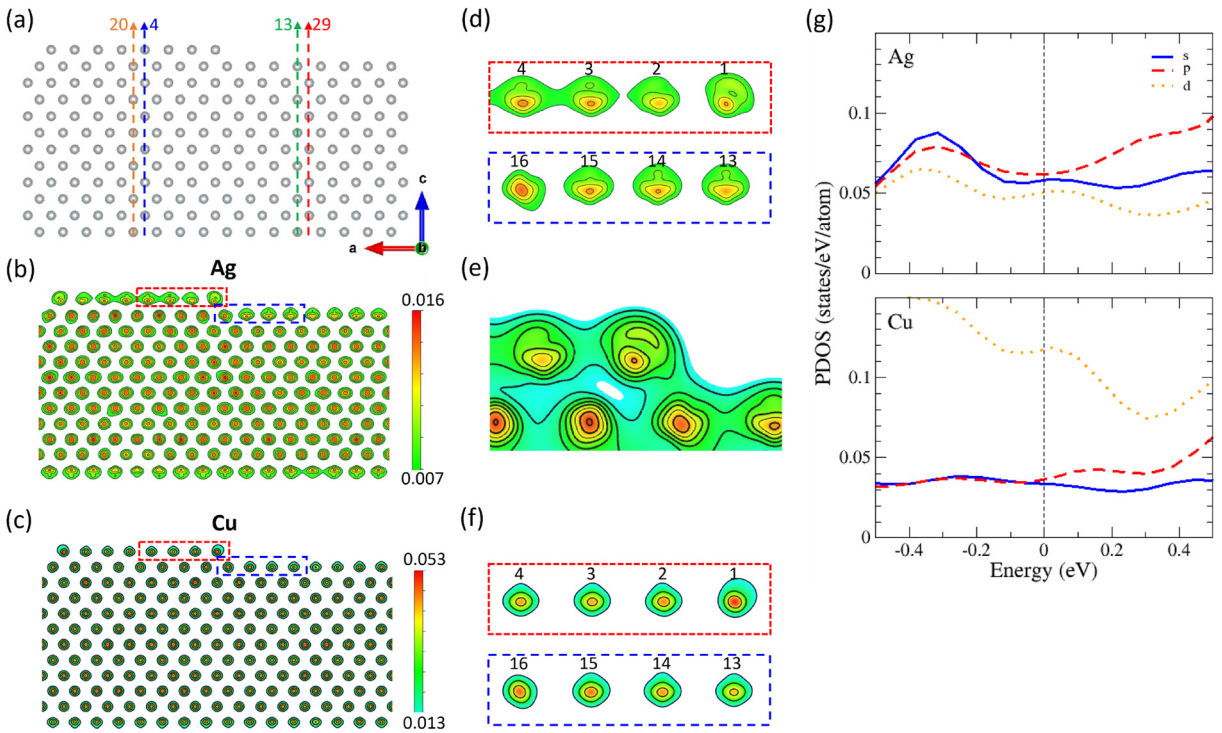

Fig. 3 (a) Side view of the step structures for both Ag and Cu. (b) and (c) Side views of electronic charge contours calculated from −0.5 eV to 0 eV (Fermi energy) for Ag and Cu, respectively. The color bar indicates charge density (e Å^{-3}). (d) Surface charge contour with interval of 0.0013, zoomed in on the atoms (marked by numbers) within the red and blue dashed rectangles in (b). (e) Calculated electronic charge contours around the step edge of Ag, consistent with (d). (f) Surface charge contour with interval of 0.0013, zoomed in on the atoms within the red and blue dashed rectangles in (c). (g) Orbital-resolved density of states for Ag and Cu at site 4. The higher density of states of Cu around the Fermi level leads to higher charge density in (c) compared to that in (b) for Ag.

that at the high terrace, the electron density decreases as the site approaches the USE (from site 4 to site 1). Conversely, at the low terrace, the electron density at the SB site (site 16) is the highest and gradually decreases with increasing distance from the SB (from site 16 to site 13). This behavior in which Ag electrons at the USB (site 1) migrate significantly toward the SB (site 16) shown in Fig. 3(e) is consistent with the Smoluchowski effect[15] illustrated schematically in Fig. 1. In contrast, Fig. 3(f) demonstrates that the surface charge distribution of Cu is relatively localized and symmetric across atoms from site 4 to site 1 on the high terrace and from site 16 to site 13 on the low terrace. It shows no indication of electron migration and displays nearly identical charge distribution for site 1 and site 16.

By comparing the charge distribution maps, we infer that the Ag-stepped surface exhibits polarization characteristics, whereas the Cu-stepped surface does not, in agreement with experimental observations in Fig. 2. Therefore, in practice, the strength of the Smoluchowski effect[15] can vary substantially between different materials. To further investigate the origin of this difference between Ag and Cu, we analyzed the orbital-resolved density of states (DOS) at the surface sites, as shown in Fig. 3(g). Near the Fermi level, the electronic states at the Ag surface primarily originate from a mixture of the diffusive 5s, 5p, and 4d orbitals, providing a strong deformation of the electron cloud, whereas those at the Cu surface are predominantly derived from the highly localized 3d orbitals with much stiffer orbital shapes. As a result, the electronic states on the Cu-stepped surface exhibit minimal deformation, and no electron transfer is observed from the USE to the SB. These findings suggest that orbital localization is the key factor determining surface polarization at stepped surfaces.

Next, we used FER1 from Fig. 2(c) and (f) to quantitatively analyze how the step influences the FER energy, as shown in Fig. 4(a) and (b), where the positions of the USE are set as zero points. For FER1 on Ag(100), depicted in Fig. 4(a), the energy is discontinuous at the step, with shifts of 0.152 eV on the high terrace and −0.123 eV on the low terraces. In contrast, for FER1 around the step on Cu(100), shown in Fig. 4(b), the energy discontinuity is absent, although a similar trend of energy shifts is observed. Notably, the energy shift on the low terrace (−0.076 eV) is approximately half of that on Ag(100). However, the energy shift on the high terrace (0.014 eV) is substantially smaller than that on Ag(100) by an order of magnitude. This uneven behavior prompted us to investigate whether it is entirely related to the SED, which is significant on Ag(100) but absent on Cu(100), as confirmed by DFT calculations.

Previous studies[50] have shown that the energy E_n of FER1, FER2, the third-order FER follows

$$E_n = E_v + \alpha F_{FER}^{\frac{2}{3}}\left(n - \frac{1}{4}\right)^{\frac{2}{3}} \quad (1)$$

in the triangular potential model, where E_v is the vacuum level, F_{FER} is the electric field responsible for FER formation, n = 1, 2, 3 corresponds to the order number, and $\alpha = \left(\frac{\hbar^2}{2m}\right)^{\frac{1}{3}}\left(\frac{3\pi e}{2}\right)^{\frac{2}{3}}$.

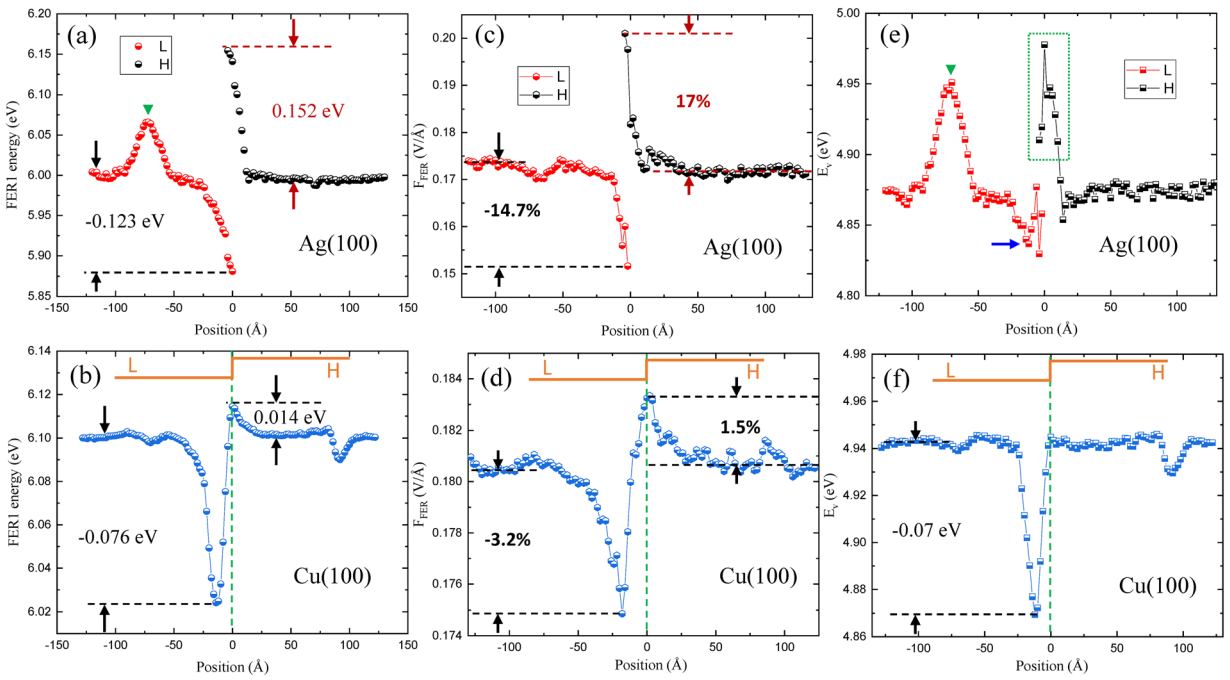

Fig. 4 (a) FER1 energies from Fig. 2(c) plotted as a function of position, with the USE set as the zero point, showing that near the step on the Ag(100), the FER1 shifts toward lower energies on the low terrace (marked by L) and higher energy on the high terrace (marked by H). (b) FER1 energies from Fig. 2(f) plotted as a function of position on the Cu(100), showing no discontinuity. (c) and (d) F_{FER} values extracted from Fig. 2(c) and (f), respectively, plotted as a function of position on Ag(100) and Cu(100). (e) and (f) E_v values obtained from Fig. 2(c) and (f), respectively, plotted as a function of position on Ag(100) and Cu(100).

Therefore, using the energies of FER1 and FER2, both E_v and F_{FER} can be determined. Fig. 4(c) displays the plot of F_{FER} extracted from Fig. 2(c) as a function of position on Ag(100), revealing that F_{FER} is discontinuous at the step. Given the positive polarity on the sample, the surface charge density σ beneath the tip is also positive, and can be expressed as $F_{FER}\varepsilon_0$, where ε_0 is the vacuum permittivity. Relative to the surface charge density σ_0 at positions away from the step, σ at the USE (σ_{USE}) is 17% higher on Ag(100), as shown in Fig. 4(c). Similarly, Fig. 4(d) shows that σ_{USE} on Cu(100) exceeds σ_0 by only 1.5%. Fig. 4(e) and (f) present the corresponding plots of E_v *versus* position on Ag(100) and Cu(100), respectively. These plots indicate that E_v remains nearly unchanged at the USE on Cu(100), whereas on Ag(100), E_v substantially increases as the USE is approached.

A work function difference can induce charge transfer due to Fermi level alignment, resulting in the creation of a contact potential, which corresponds to the vacuum level difference. Conversely, charge transfer can also lead to changes in the work function (vacuum level). Since the SED arises from charge transfer from the USE to the SB (Fig. 1), the Fermi level near SB (USE) is higher (lower) than that away from the step, as illustrated in Fig. 5(a). However, because the Fermi level must align across the surface, this implies that the vacuum level is discontinuous at the step, being higher at the USE with a positive charge density, as depicted in Fig. 5(b). Based on this perspective, the absence of changes at the USE in Fig. 4(f) results from that no charge transfer occurs at the step on Cu(100). In contrast, Fig. 4(e) reveals a clear discontinuity at the step on Ag(100), indicating significant charge transfer. These observations align with the results of DFT calculations. As shown in Fig. 5(b), negative charge density leads to a lower vacuum level, consistent with an FER study on nitrogen-doped graphene,[51] where the nitrogen atom exhibits a lower vacuum level than pristine graphene due to the additional electron accumulating around the nitrogen atom.

Although the USE on Cu(100) is neutral, Fig. 4(d) shows a detectable variation (1.5%) in F_{FER} at the USE, which can be attributed to the geometric structure of the step, as illustrated in Fig. 5(c). In this figure, position T (T') indicates that the tip is positioned away from the step on the high (low) terrace. When the tip approaches the USE, the average distance between the tip and the surface becomes larger than at T due to the step geometry. This results in a lower current because the electric field for field emission, F_{FE}, is weaker at the same bias voltage. To compensate, the STM feedback mechanism drives the tip closer to the high terrace to maintain the same current (F_{FE}), thereby increasing F_{FER} at the USE compared to T. Conversely, when the tip approaches the SB, it moves away from the low terrace, reducing F_{FER} relative to T'. As the tip moves from the low terrace to the high terrace, crossing the step on Cu(100), F_{FER} decreases gradually to a minimum, then reverses to a maximum, followed by a gradual reduction, as shown in Fig. 4(d). However, the change relative to the minimum is −3.2%, indicating that the step has more pronounced effect on F_{FER} at the low terrace. This change is considerably smaller than that (−14.7%) on Ag(100). Fig. 4(c) and (d) reveals that the charge transfer at the step on Ag(100) is substantially more drastic than that on Cu(100), in agreement with the calculated results in Fig. 3(d) and (f).

Our previous study demonstrated that E_v can vary linearly with F_{FER}, with a mean slope of approximately 6.8 eV Å V^{-1}, due to the tip-induced local Fermi level alignment.[52] Using this slope, the variations in E_v (ΔE_v) corresponding to Fig. 4(d) relative to the rightmost point are calculated and shown in Fig. 5(d), where ΔE_v for Fig. 4(f) is also depicted for comparison. Fig. 5(d) reveals a discrepancy between the two plots, suggesting that E_v may not change with F_{FER} in this case. We have also demonstrated that E_v depends on the average charge density $\bar{\sigma}$ over the surface area beneath the tip apex, rather than directly on σ, which is proportional to F_{FER}.[52] When the tip crosses the step, the average negative charge density at the tip apex should remain unchanged to maintain a constant field emission current. This mechanism can preserve a constant $\bar{\sigma}$ beneath the tip apex even as it moves across the step. Thus, the dip feature (0.07 eV depth) at the low terrace in Fig. 4(f) is not induced by the electric field in the STM junction but is an intrinsic surface property (discussed later). This property also accounts for the 0.035 eV reduction in E_v (marked by an arrow) in Fig. 4(e). Due to the SED on Ag(100), $\bar{\sigma}$ is not constant and increases near the USE because of additional positive charge density, leading to a rise of E_v in Fig. 4(e). After reaching a

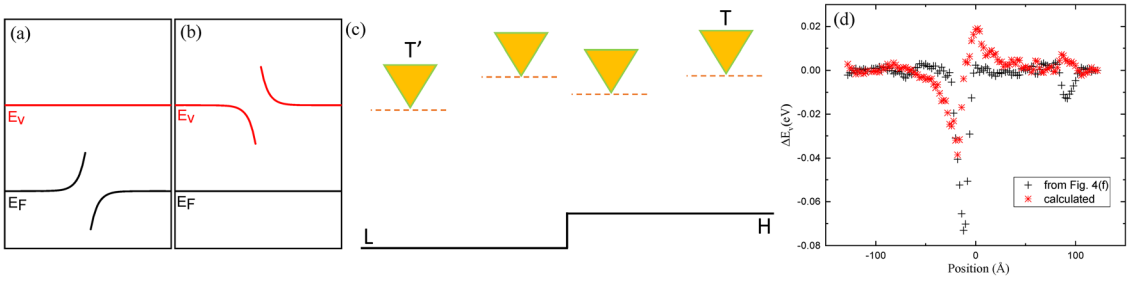

Fig. 5 (a) The Fermi level near SB (USE) is higher (lower) than that far from the step due to charge transfer. (b) The Fermi level must align across the surface, resulting in a discontinuity of the vacuum level at the step. (c) Schematic illustration showing that near the step, the distance between the tip and the high (low) terrace is shorter (longer) than that at T (T') position away from the step. (d) The vacuum level variation ΔE_v corresponding to Fig. 4(d), is calculated relative to the rightmost point using a slope of 6.8 eV Å V^{-1}. For comparison, ΔE_v for Fig. 4(f) is also shown.

maximum at the USE, E_v begins to decline, indicating that $\bar{\sigma}$ includes the negative charge density at the SB. Consequently, the peak feature marked by a dashed rectangle may serve as a direct signal of positive and negative charge distributions within the SED. Additionally, this peak signal reveals a reversed result to a widely accepted notion that as charge transfer occurs, local positive (negative) surface charge reduces (increases) the work function.[53]

Previous studies have demonstrated that in either space[54] or energy,[55] the position of the maximum in the dI/dV signal may not coincide with the position of the maximum of the DOS. This situation likely occurs in the case of field emission resonance. However, our study focuses on F_{FER}, which is determined from the energy separation between FER1 and FER2 using eqn (1). Since F_{FER} depends on this energy separation, whether the extracted positions of FER1 and FER2 match the positions of the DOS maxima is not critical. A similar situation was reported in the study of interference waves by Li *et al.*:[54] although the observed peak positions do not coincide with the positions of the DOS maxima, the measured wavelength still agrees with the positional separation between the DOS maxima. In addition, the vacuum level determined from the energies of FER1 and FER2 may be uncertain due to this possible discrepancy between the extracted resonance positions and the positions of the DOS maxima. However, our concern is the variation in the work function, for which, this discrepancy can cancel out.

Fig. 4(f) shows that even in the absence of the SED, the step on Cu(100) still induces a work function reduction (WFR) of 0.07 eV at a distance 12 Å from the step at the low terrace. Additionally, Fig. 5(b) indicates that the work function variations induced by the SED are entirely compensated. These results clarify that the WFR observed in the previous studies[16–18] was not due to the SED. In particular, the measurements through I–Z spectroscopy of STM[17] did not reveal a work function increase at the USE, as seen in Fig. 4(e). Moreover, Fig. 4(e) also shows a WFR of 0.035 eV on Ag(100), where the SED is significant. Here, we suggest that this WFR is independent of the SED and arises from surface atom relaxation near the SB due to step formation. It is well known that the surface dipole layer (SDL) influences the work function. If the SDL is affected by local surface atomic structure, surface atom relaxation likely induces the work function change. In Fig. 2(a), the dashed line also intersects a defective area marked by an arrow. Consequently, both FER1 energy in Fig. 4(a) and E_v in Fig. 4(e) exhibit a peak characteristic (marked by a triangle) at this location, indicating that the SDL is sensitive to surface atomic structure.

4. Conclusions

In summary, we use the FER technique to demonstrate that the Smoluchowski effect is pronounced in Ag(100) but negligible in Cu(100). This finding is further supported by DFT calculations. Charge density analysis in calculations reveals that the SED does not emerge on the Cu(100) surface, owing to the strong localization of Cu-3d electrons near the Fermi level. In contrast, surface electrons near the Fermi level on Ag(100) mainly consist of diffusive 5s, 5p, and 4d orbitals, which are more responsive to perturbations from the step edge. As a result, significant charge transfer induces a polarity discontinuity at the step site, manifesting as discontinuous FER energies in Ag(100). By applying the triangular potential model to extract work functions from FER energies, we identify a peak feature in the measured work function profile near the USE. This feature provides direct evidence of the spatial distribution of positive and negative charge density within the SED, which has not yet been resolved by other local probe techniques. Furthermore, this signal confirms that local positive (negative) charge densities locally increase (decrease) the work function as the charge transfer occurs. Although the Smoluchowski effect is absent on Cu(100), a local reduction in the work function is still observed near the SB, indicating that this reduction may arise from other step-induced electronic modifications rather than from the Smoluchowski effect.

Conflicts of interest

There are no conflicts to declare.

Data availability

The authors declare that all data in this article are available upon reasonable request.

The data supporting this article have been included as part of the supplementary information (SI). The supplementary information describes the slab model used to simulate monoatomic steps on the Ag(100) and Cu(100) surfaces, the convergence tests for slab thickness, and the examinations of the influence of step orientation on the FER spectra. See DOI: https://doi.org/10.1039/d5nh00426h.

Acknowledgements

The authors are grateful for the support provided by the Academia Sinica (Grants No: AS-iMATE-113-13 and AS-iMATE-111-13) and the National Science and Technology Council (NSTC 113-2112-M-001-048 and NSTC 112-2112-M-007-034-MY3), Taiwan. H.-T. J. is also thankful for support from NCHC, CINC-NTU, and CQT-NTHU-MOE, Taiwan.

References

1 L. Romaner, G. Heimel, J. Bredas, A. Gerlach, F. Schreiber, R. L. Johnson, J. Zegenhagen, S. Duhm, N. Koch and E. Zojer, Impact of bidirectional charge transfer and molecular distortions on the electronic structure of a metal–organic interface, *Phys. Rev. Lett.*, 2007, **99**, 256801.

2 S. Bedwani, D. Wegner, M. F. Crommie and A. Rochefort, Strongly reshaped organic–metal interfaces: tetracyanoethylene on Cu(100), *Phys. Rev. Lett.*, 2008, **101**, 216105.

3 I. Fernandez-Torrente, S. Monturet, K. J. Franke, J. Fraxedas, N. Lorente and J. I. Pascual, Long-range repulsive interaction between molecules on a metal surface induced by charge transfer, *Phys. Rev. Lett.*, 2007, **99**, 176103.
4 C. Urban, Y. Wang, J. Rodríguez-Fernández, R. García, M. A. Herranz, M. Alcamí, N. Martín, F. Martín, J. M. Gallego, R. Miranda and R. Otero, Charge transfer-assisted self-limited decyanation reaction of TCNQ-type electron acceptors on Cu(100), *Chem. Commun.*, 2014, **50**, 833.
5 A. Zhao, Q. Li, L. Chen, H. Xiang, W. Wang, S. Pan, B. Wang, X. Xiao, J. Yang, J. G. Hou and Q. S. Zhu, Controlling the Kondo effect of an adsorbed magnetic ion through its chemical bonding, *Science*, 2005, **309**, 1542.
6 V. Iancu, A. Deshpande and S.-W. Hla, Manipulating Kondo temperature via single molecule switching, *Nano Lett.*, 2006, **6**, 820.
7 Z. L. Wang, From contact electrification to triboelectric nanogenerators, *Rep. Prog. Phys.*, 2021, **84**, 096502.
8 W. Melitz, J. Shen, A. C. Kummel and S. Lee, Kelvin probe force microscopy and its application, *Surf. Sci. Rep.*, 2011, **66**, 1.
9 B. Hendriksen, M. Ackermann and R. van Rijn, *et al.*, The role of steps in surface catalysis and reaction oscillations, *Nat. Chem.*, 2010, **2**, 730.
10 A. Riemann, S. Fölsch and K. H. Rieder, Epitaxial growth of alkali halides on stepped metal surfaces, *Phys. Rev. B: Condens. Matter Mater. Phys.*, 2005, **72**, 125423.
11 N. Reinecke, S. Reiter, S. Vetter and E. Taglauer, Steps, facets and nanostructures: investigations of Cu(11n) surfaces, *Appl. Phys. A: Mater. Sci. Process.*, 2002, **75**, 1.
12 E. A. Carbonio, M. J. Prieto, A. de Siervo and R. Landers, From 1D to 3D Ru nanostructures on a Pt stepped surface as model systems in electrocatalysis: UHV-STM and XPS study, *J. Phys. Chem. C*, 2014, **118**, 28679.
13 G. Ehrlich and F. G. Hudda, Atomic view of surface self-diffusion: tungsten on tungsten, *J. Chem. Phys.*, 1966, **44**, 1039.
14 R. L. Schwoebel, Step motion on crystal surfaces, *J. Appl. Phys.*, 1969, **40**, 614.
15 R. Smoluchowski, Anisotropy of the electronic work function of metals, *Phys. Rev.*, 1941, **60**, 661.
16 H. Besocke, B. Krahl-Urban and H. Wagner, Dipole moments associated with edge atoms; a comparative study on stepped Pt, Au and W surfaces, *Surf. Sci.*, 1977, **68**, 39.
17 J. F. Jia, K. Inoue, Y. Hasegawa, W. S. Yang and T. Sakurai, Variation of the local work function at steps on metal surfaces studied with STM, *Phys. Rev. B: Condens. Matter Mater. Phys.*, 1998, **58**, 1193.
18 K. M. Burson, Y. Wei, W. G. Cullen, M. S. Fuhrer and J. E. Reutt-Robey, Potential steps at C60–TiOPc–Ag(111) interfaces: ultrahigh-vacuum-noncontact scanning probe metrology, *Nano Lett.*, 2012, **12**, 2859.
19 J. Y. Park, G. M. Sacha, M. Enachescu, D. F. Ogletree, R. A. Ribeiro, P. C. Canfield, C. J. Jenks, P. A. Thiel, J. J. Sáenz and M. Salmeron, Sensing dipole fields at atomic steps with combined scanning tunneling and force microscopy, *Phys. Rev. Lett.*, 2005, **95**, 136802.
20 K. H. Gundlach, Zur berechnung des tunnelstroms durch eine trapezformige potentialstufe, *Solid-State Electron.*, 1966, **9**, 949.
21 G. Binnig, K. H. Frank, H. Fuchs, N. Garcia, B. Reihl, H. Rohrer, F. Salvan and A. R. T. Williams, Tunneling spectroscopy and inverse photoemission - image and field states, *Phys. Rev. Lett.*, 1985, **55**, 991.
22 R. S. Becker, J. A. Golovchenko and B. S. Swartzentruber, Electron interferometry at crystal-surfaces, *Phys. Rev. Lett.*, 1985, **55**, 987.
23 K. Bobrov, A. J. Mayne and G. Dujardin, Atomic-scale imaging of insulating diamond through resonant electron injection, *Nature*, 2001, **413**, 616.
24 C. G. Yue, Z. Q. Huang, W. L. Wang, Z. A. Gao, H. C. Lin, J. W. Liu and K. Chang, Identification and manipulation of atomic defects in monolayer SnSe, *ACS Nano*, 2024, **18**, 25478.
25 P. S. N. Barimar, B. Naydenov, J. Li and J. J. Boland, Spreading resistance at the nano-scale studied by scanning tunneling and field emission spectroscopy, *Appl. Phys. Lett.*, 2017, **110**, 263111.
26 C. L. Lin, S. M. Lu, W. B. Su, H. T. Shih, B. F. Wu, Y. D. Yao, C. S. Chang and T. T. Tsong, Manifestation of work function difference in high order Gundlach oscillation, *Phys. Rev. Lett.*, 2007, **99**, 216103.
27 P. Yang, M. Y. Zhao, X. Y. Ran, C. Zhang, W. Q. Luo, W. Y. Sun, J. Xie, D. Y. Cao and J. Guo, Identifying the structure of two-dimensional ACu6O5 (A = Na, K, Cs) film on Cu(111) with atomic resolution, *J. Phys. Chem. Lett.*, 2025, **16**, 1038.
28 A. Kumar, K. Banerjee, M. M. Ervasti, S. Kezilebieke, M. Dvorak, P. Rinke, A. Harju and P. Liljeroth, Electronic characterization of a charge-transfer complex monolayer on graphene, *ACS Nano*, 2021, **15**, 9945.
29 C. Gutiérrez, L. Brown, C. J. Kim, J. Park and A. N. Pasupathy, Klein tunneling and electron trapping in nanometre-scale graphene quantum dots, *Nat. Phys.*, 2016, **12**, 3806.
30 Q. Zhang, J. Yu, P. Ebert, C. Zhang, C. R. Pan, M. Y. Chou, C. K. Shih, C. Zeng and S. Yuan, Tuning band gap and work function modulations in monolayer hBN/Cu(111) heterostructures with moiré patterns, *ACS Nano*, 2018, **12**, 9355.
31 B. Borca and H. J. W. Zandvliet, Image potential states of 2D materials, *Appl. Mater. Today*, 2024, **39**, 102304.
32 Q. Wu, W. Quan, S. Pan, J. Hu, Z. Zhang, J. Wang, F. Zheng, Y. Zhang and J. Wang, Atomically thin kagome-structured Co9Te16 achieved through self-intercalation and its flat band visualization, *Nano Lett.*, 2024, **24**, 7672.
33 Z.-Q. Fu, Y. Pan, J.-J. Zhou, K.-K. Bai, D.-L. Ma, Y. Zhang, J.-B. Qiao, H. Jiang, H. Liu and L. He, Relativistic artificial molecules realized by two coupled graphene quantum dots, *Nano Lett.*, 2020, **20**, 6738.
34 W. B. Su, S. M. Lu, C. L. Lin, H. T. Shih, C. L. Jiang, C. S. Chang and T. T. Tsong, Interplay between transmission background and gundlach oscillation in scanning tunneling spectroscopy, *Phys. Rev. B: Condens. Matter Mater. Phys.*, 2007, **75**, 195406.

35 Y. Girard, S. Benbouabdellah, O. Chahib, C. Chacon, A. Bellec, V. Repain, J. Lagoute, Y. J. Dappe, C. González and W. B. Su, Growth and local electronic properties of cobalt nanodots underneath graphene on SiC(0001), *Carbon*, 2023, **208**, 22.

36 W. B. Su, C. L. Lin, W. Y. Chan, S. M. Lu and C. S. Chang, Field enhancement factors and self-focus functions manifesting in field emission resonances in scanning tunneling microscopy, *Nanotechnology*, 2016, **27**, 175705.

37 S. V. Korachamkandy, S. M. Lu, W. B. Su, W. Y. Chan, H. H. Chang, H. T. Jeng, C. H. Lee and C. S. Chang, Probing tip-induced attractive deformation of graphite surfaces through wave function dissipation in field emission resonance, *J. Phys. Commun.*, 2022, **6**, 075010.

38 S. V. Korachamkandy, S. M. Lu, W. Y. Chan, H. H. Chang, C. H. Lee and W. B. Su, Characterization of apex structures of scanning tunneling microscope tips with field emission resonance energies, *Jpn. J. Appl. Phys.*, 2022, **61**, 085001.

39 A. Schlenhof, G. C. Kokkorakis and J. P. Xanthakis, High-order gundlach resonances at exceptionally large voltages: consequences for determining work functions, *Appl. Phys. Lett.*, 2022, **120**, 261601.

40 A. Y. Aladyshkin and K. Schouteden, Field-emission resonances in thin metallic films: nonexponential decrease of the tunneling current as a function of the sample-to-tip distance, *J. Phys. Chem. C*, 2022, **126**, 13341.

41 K. Chang, J. W. D. Villanova, J. R. Ji, S. Das, F. Küster, S. Barraza-Lopez, P. Sessi and S. S. P. Parkin, Vortex-oriented ferroelectric domains in SnTe/PbTe monolayer lateral heterostructures, *Adv. Mater.*, 2021, **33**, 2102267.

42 W. B. Su, S. M. Lu, H. T. Jeng, W. Y. Chan, H. H. Chang, W. W. Pai, H. L. Liu and C. S. Chang, Observing quantum trapping on MoS_2 through the lifetimes of resonant electrons: revealing the Pauli exclusion principle, *Nanoscale Adv.*, 2020, **2**, 5848.

43 P. Hohenberg and W. Kohn, Inhomogeneous electron gas, *Phys. Rev.*, 1964, **136**, B864.

44 W. Kohn and L. J. Sham, Self-consistent equations including exchange and correlation effects, *Phys. Rev.*, 1965, **140**, A1133.

45 G. Kresse and J. Hafner, Ab initio molecular dynamics for open-shell transition metals, *Phys. Rev. B: Condens. Matter Mater. Phys.*, 1993, **48**, 13115.

46 G. Kresse and J. Furthmüller, Efficient iterative schemes for ab initio total-energy calculations using a plane-wave basis set, *Phys. Rev. B: Condens. Matter Mater. Phys.*, 1996, **54**, 11169.

47 G. Kresse and D. Joubert, From ultrasoft pseudopotentials to the projector augmented-wave method, *Phys. Rev. B: Condens. Matter Mater. Phys.*, 1999, **59**, 1758.

48 P. A. Ignatiev, *et al.*, Electronic confinement on stepped Cu(111) surfaces: ab initio study, *Phys. Rev. B: Condens. Matter Mater. Phys.*, 2007, **75**, 155428.

49 W. P. Davey, Precision measurements of the lattice constants of twelve common metals, *Phys. Rev.*, 1925, **25**, 753.

50 W. B. Su, S. M. Lu, H. H. Chang, H. T. Jeng, W. Y. Chan, P. C. Jiang, K. H. Lin and C. S. Chang, Impact of band structure on wave function dissipation in field emission resonance, *Phys. Rev. B*, 2022, **105**, 195411.

51 J. Neilson, H. Chinkezian, H. Phirke, A. Osei-Twumasi, Y. Li, C. Chichiri, J. Cho, K. Palotas, L. Gan, S. J. Garrett, K. C. Lau and L. Gao, Nitrogen-doped graphene on copper: edge-guided doping process and doping-induced variation of local work function, *J. Phys. Chem. C*, 2019, **123**, 8802.

52 W. B. Su, W. Y. Chan, S. M. Lu, H. H. Chang and C. S. Chang, Tip-induced local Fermi level alignment: a stark shift in vacuum level in scanning tunneling microscope configurations, *Chin. J. Phys.*, 2024, **92**, 877.

53 B. Di, Z. Peng, Z. Wu, X. Zhou and K. Wu, Spatially resolved and quantitatively revealed charge transfer between single atoms and catalyst supports, *J. Mater. Chem. A*, 2022, **10**, 5889.

54 J. Li, W.-D. Schneider and R. Berndt, Local density of states from spectroscopic scanning-tunneling-microscope images: Ag (111), *Phys. Rev. B: Condens. Matter Mater. Phys.*, 1997, **56**, 7656.

55 M. Ziegler, N. Néel, A. Sperl, J. Kröger and R. Berndt, Local density of states from constant-current tunneling spectra, *Phys. Rev. B: Condens. Matter Mater. Phys.*, 2009, **80**, 125402.